PAPER

Measurements and modelling of fast-ion redistribution due to resonant MHD instabilities in MAST

IOP Publishing Plasma Physics and Controlled Fusion
Plasma Phys. Control. Fusion **57** (2015) 125009 (17pp) doi:10.1088/0741-3335/57/12/125009

Measurements and modelling of fast-ion redistribution due to resonant MHD instabilities in MAST

O M Jones[1,2], M Cecconello[3], K G McClements[2], I Klimek[3], R J Akers[2], W U Boeglin[4], D L Keeling[2], A J Meakins[2], R V Perez[4], S E Sharapov[2], M Turnyanskiy[5] and the MAST team[2]

[1] Department of Physics, Durham University, South Road, Durham DH1 3LE, UK
[2] CCFE, Culham Science Centre, Abingdon, Oxfordshire OX14 3DB, UK
[3] Department of Physics and Astronomy, Uppsala University, SE-751 05 Uppsala, Sweden
[4] Department of Physics, Florida International University, 11200 SW 8 ST, CP204, Miami, FL 33199, USA
[5] ITER Physics Department, EUROfusion PMU Garching, Boltzmannstraße 2, D-85748 Garching, Germany

E-mail: owen.jones@ccfe.ac.uk

Received 23 March 2015, revised 9 September 2015
Accepted for publication 28 September 2015
Published 3 November 2015

Abstract

The results of a comprehensive investigation into the effects of toroidicity-induced Alfvén eigenmodes (TAE) and energetic particle modes on the NBI-generated fast-ion population in MAST plasmas are reported. Fast-ion redistribution due to frequency-chirping TAE in the range 50 kHz–100 kHz and frequency-chirping energetic particle modes known as fishbones in the range 20 kHz–50 kHz, is observed. TAE and fishbones are also observed to cause losses of fast ions from the plasma. The spatial and temporal evolution of the fast-ion distribution is determined using a fission chamber, a radially-scanning collimated neutron flux monitor, a fast-ion deuterium alpha spectrometer and a charged fusion product detector. Modelling using the global transport analysis code TRANSP, with *ad hoc* anomalous diffusion and fishbone loss models introduced, reproduces the coarsest features of the affected fast-ion distribution in the presence of energetic particle-driven modes. The spectrally and spatially resolved measurements show, however, that these models do not fully capture the effects of chirping modes on the fast-ion distribution.

Keywords: diagnostics, fast-ion population, Alfvén eigenmodes, fishbones, spherical tokamak

(Some figures may appear in colour only in the online journal)

1. Introduction

The behaviour of energetic ions in tokamak plasmas is an important topic of study for two principal reasons [1]: fast ions provide a substantial part of the plasma heating in current fusion experiments, hence their confinement is necessary in order to maintain high electron and ion temperatures; and fast ions lost through the plasma boundary may impact the first wall of the device, causing damage to plasma-facing components. This effect is particularly significant for toroidally-localised structures such as radio-frequency heating antennae, which may be exposed to highly localised heat loads. For these reasons, it is crucial to study the enhanced transport of fast ions, which is known to be caused by a wide range of magnetohydrodynamic (MHD) instabilities in tokamak plasmas.

The mega-amp spherical tokamak (MAST) was reliant on neutral beam heating, which constitutes a source of energetic ions, to access high-performance operating regimes [2, 3]. One of the world's largest spherical tokamaks to date, typical parameters of MAST were: major and minor radius $R = 0.95$ m, $a = 0.60$ m; plasma current $I_p = 400$–900 kA; toroidal field on axis $B_T = 0.40$–0.58 T; core electron density

and temperature $n_{e0} = 3 \times 10^{19}$ m^{-3}and $T_{e0} = 1$ keV. The neutral beam injection (NBI) system installed on the MAST consisted of two positive ion sources capable of accelerating deuterons to energies of 75 keV. Each injector could deliver up to 2.5 MW of power when tuned to optimum perveance [4]. Deuterium beam injection into deuterium plasmas was most commonly used on MAST, and such plasmas are the subject of this paper.

Fast ions (FIs) in MAST were produced by the ionisation of beam neutrals as they propagated through the plasma. The relatively weak magnetic field resulted in large Larmor radii of up to 10 cm for the highest energy beam ions. Once they are deposited, FIs interact with the background plasma, slowing down by electron drag and scattering off thermal ions. Ultimately, the ions may either: thermalise, reaching equilibrium with the background plasma; undergo fusion reactions, producing a triton and proton, or ^{3}He nucleus and neutron; become reneutralised by charge exchange with beam or thermal neutrals; collisionally scatter onto unconfined orbits; or be lost from the plasma due to instabilities or static field perturbations. In order to maximise the electron and ion heating and fraction of the NBI-driven current in the plasma, and hence measures of performance such as plasma beta, it is desirable to confine the FIs for as long as possible. Maximising the fraction of the NBI-driven current requires these ions to be confined at low plasma density, posing challenges for avoiding energetic particle-driven instabilities. Diagnosing the behaviour of FIs in MAST and establishing the mechanisms for their redistribution within and loss from the plasma are the objectives of the present study.

This paper focuses specifically on the transport of FIs in MAST caused by MHD instabilities which resonate with them [5]. This resonant interaction allows significant energy transfer from the FI population to the MHD mode in the linear growth phase. Subsequent nonlinear evolution of the mode is typically associated with the large-scale coherent transport of the resonant FI [6]. The mode acts to flatten the FI distribution close to the resonance in real space and in velocity space. In the worst-case scenario, where several resonances overlap or where sufficient free energy is present in the FI distribution to drive the mode over a spatially-extended region, FIs may even be transported to the plasma boundary and lost.

The two FI-resonant instabilities most commonly observed in MAST were frequency-chirping toroidal Alfvén eigenmodes (TAEs), and fishbones. Chirping TAEs appeared at a frequency corresponding to the toroidicity-induced gap in the Alfvén continuum in the core of the plasma, at around 100 kHz, and swept rapidly downward to approximately 50 kHz over 1–2 ms. They occurred early in the discharge, during the current ramp, and started around 10 ms after the first application of NBI. Prior numerical analysis has revealed the TAEs in MAST to be global modes, extending from the axis to a radial location close to the edge of the plasma [7]. Fishbones occurred later in MAST discharges, during the plasma current flat-top phase, and tended to occur quasi-periodically. Individual bursts typically lasted 3–4 ms and chirped down in frequency from 50 kHz–20 kHz during this time. These modes are closely related to the ideal-MHD internal kink and consist primarily of a rigid deformation of the region inside the safety factor $q = 1$ magnetic flux surface.

MAST provided a useful facility for the study of energetic-particle physics for a number of reasons. Foremost among these were the super-Alfvénic beam ions, which allowed Alfvén eigenmodes to be driven via the fundamental resonance $v_\parallel = v_A$, and the large orbit widths of the FIs, which pose a challenge to the verification of numerical models [8]. MAST was therefore equipped with a number of advanced diagnostics designed to probe the dynamics of the beam-ion population. Recent work by many of the present authors [7] has highlighted the complementary nature of the different FI diagnostics installed on MAST, presenting an overview of the observed FI transport in the presence of chirping TAEs, fishbones, sawteeth and the long-lived internal kink mode. This paper forms a natural continuation of that study, and aims to provide a quantitative verification of the key results presented in the prior work. The main findings are the confirmation that anomalous transport and losses of FIs accompany both chirping TAEs and fishbones; the demonstration that multiple diagnostic signals may in some cases be modelled consistently using anomalous FI diffusion in a global transport model; and the identification of the passing FI population in the core of the plasma as being susceptible to redistribution in the presence of fishbones. This work expands upon the previous study by providing:

- a rigorous quantitative assessment of the degree to which the reduction in FI confinement is correlated with TAEs and fishbones;
- direct experimental confirmation of the fact that these MHD modes cause losses of FIs from the plasma;
- an improved implementation of the fishbone loss model in TRANSP, including fast-ion deuterium alpha (FIDA) data as a constraint for the first time;
- a demonstration that simultaneous analysis of data from multiple FI diagnostics allows transport models to be confronted and validated, or to have their shortcomings revealed.

Section 2 of this paper describes the FI diagnostics used in this study. The plasma scenarios investigated in the course of this study are outlined in section 3. Sections 4 and 5 present the experimental results and associated FI transport modelling. This modelling was performed with the 1.5-dimensional (1D profiles mapped onto a 2D equilibrium grid), time-dependent transport analysis code TRANSP [9]. The Monte Carlo particle-tracking module NUBEAM [10] was used to model the deposition and orbits of the FIs and to generate local FI distributions as a function of energy and pitch. The main conclusions of the work are presented in section 6.

2. Fast-ion diagnostics on the MAST

2.1. Description of the diagnostics

During the 2013 MAST experimental campaign, four FI diagnostics were available on the device; one of these,

the *charged fusion product detector* (CFPD), is a novel prototype diagnostic, which was only installed for a limited period [11]. The other three diagnostics are: a uranium-235 fission chamber for volume-integrated neutron flux measurements [12]; a collimated, radially-scanning neutron detector (known as the neutron camera, or NC) [13]; and a dual-view fast-ion deuterium alpha (FIDA) diagnostic [14]. Figure 1 shows the detector positions and lines of sight of each of these diagnostics projected onto the poloidal and equatorial planes of MAST vessel.

It should be noted that although measurements of the neutron flux are not fundamentally restricted to FI diagnostic applications, the relatively low ion temperature in MAST plasmas (typically $T_i \lesssim 2$ keV in the core of the plasma) resulted in a very low contribution of thermonuclear fusion reactions to the total neutron yield. Approximately 98% of D–D fusion reactions in the MAST occurred either between a beam ion and a thermal ion (∼80%), or between two beam ions (∼20%). As a result, the flux of 2.45 MeV neutrons leaving the plasma provided information about the non-thermal, high-energy part of the deuterium ion velocity distribution. The ^{235}U fission chamber, or FC [12], measured the volume-integrated neutron flux from the plasma with a temporal resolution of 10 μs, while the NC had four collimated lines of sight (LOS) allowing the detectors to view the plasma through a thin flange in MAST vacuum vessel [13]. Two of the LOS lay in the machine midplane, and the other two were oriented diagonally downward such that at the point of their tangency to the flux surfaces they lay approximately 20 cm below the midplane. The NC assembly was mounted on a curved rail, allowing the LOS to be scanned across the plasma between discharges; repeated discharges allowed a neutron emission profile, integrated within the NC fields of view, to be obtained as a function of viewing tangency radius. Data are typically integrated over 1 ms, setting the temporal resolution of the measurements.

The CFPD was installed on MAST to provide a complementary measurement to that provided by the NC [11]. Four detectors measured the flux of 3.02 MeV protons and 1.01 MeV tritons (the gyro-radii of these two fusion products being very nearly equal) produced by D–D fusion reactions. Collimators in the protective casing allowed fusion products to reach the detectors, and an aluminium foil prevented detection of soft x-rays. The diagnostic was mounted on the end of a linear reciprocating probe inserted into MAST vessel at the midplane. This diagnostic technique is practical in small, low-field devices such as MAST because the large gyro-radii of the fusion products render them essentially unconfined by the magnetic field; they leave the plasma within a single gyro-orbit. With a suitable equilibrium reconstruction, the orbits of these particles may be tracked 'backward in time' from the detector to determine the possible location of their emission. Retraction or insertion of the probe between repeated discharges allowed a spatial scan of the proton/triton emission profile. Protons and tritons are discriminated in post-processing. As in the case of the NC, the integration time of the data is typically set to 1 ms.

The FIDA diagnostic provided a measurement of the FI density by observing the Balmer-alpha (D_α) emission of reneutralised fast deuterons which had undergone charge exchange (CX) with beam or halo neutrals [14]. *Halo neutrals* are thermal neutrals created by CX between beam neutrals and thermal ions. The light was coupled via optical fibres to a spectrometer, and spectral resolution was provided by the dispersion of a bandpass-filtered portion of this light. Spatial resolution was obtained by using individual fibres for each LOS through the plasma. The spectrum of FIDA light provides information about the distribution of the LOS velocity of the FI at the point at which CX occurred; D_α light from reneutralised ions moving away from the lens is red-shifted, while that from ions moving toward the lens is blue-shifted. Eleven channels could be connected to the spectrometer at any given time, allowing a radial profile of the FIDA emission to be acquired within a single discharge. Data were acquired with 0.3 ms temporal resolution. Two sets of views were available: a near-toroidal set from a lens mounted just above the vessel midplane, and a near-vertical set from a lens mounted inside the vessel, looking vertically downwards at the neutral beam. The toroidal views were predominantly sensitive to passing FIs, with a large pitch $p = v_\parallel/v$, while the vertical views were more sensitive to trapped FIs with smaller values of pitch. Only data from the toroidal views are used in this study, since the light throughput of the vertical views was insufficient to allow small, rapid changes in FIDA emission to be identified.

An example of the data from each of the diagnostics described in this section is shown in figure 2. 2.0 MW of neutral beam heating power (at $E_b = 70$ keV) was applied from 0.051 s, with an additional 0.7 MW (at $E_b = 44$ keV) applied from 0.101 s. A series of large fishbones occurred between 0.20 s–0.25 s; the time of the first of these bursts of MHD activity is indicated by the dashed vertical line. The effect of the fishbones is apparent as a significant drop in the magnitude of the signal in each time trace; this effect is particularly marked in the NC, FIDA and CFPD data, where drops in excess of 25% of the pre-fishbone signal are observed.

3. Plasma scenarios

For the purposes of this study, two sets of discharges were selected for the analysis of the effects of fishbones and TAEs on the FI population. Both sets consist of discharges with high NBI power and high electron density, the combination of which provides a reasonable signal-to-noise ratio (SNR) in the FI diagnostic signals along with large-amplitude bursts of TAEs and fishbones separated in time by approximately 5–10 ms. These points are important in allowing the effects of individual bursts of MHD activity on the FI population to be resolved by each diagnostic. A further reason for choosing these discharges is the fact that the NC was scanned in tangency radius between repeated shots, allowing composite NC count-rate profiles to be derived.

Figure 3 shows time traces of key parameters related to the FI population and MHD activity in a representative discharge from each of the two sets analysed in the course of this

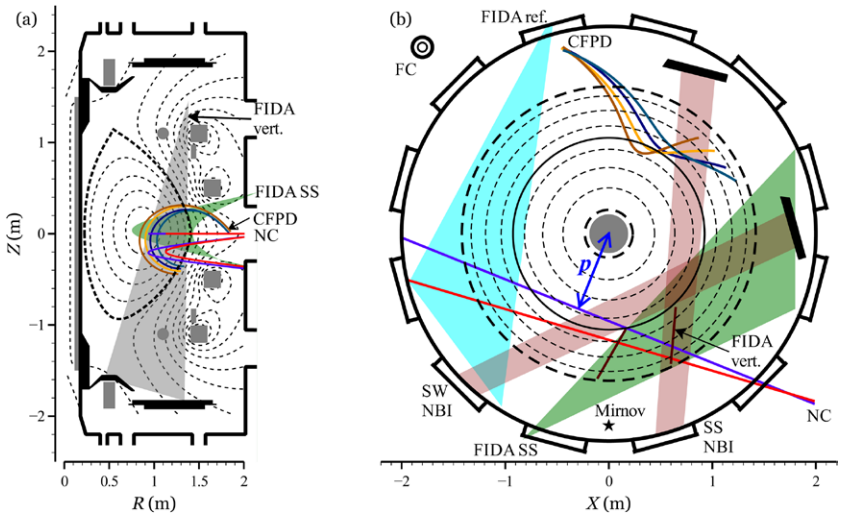

Figure 1. Poloidal (a) and equatorial (b) projections of the viewing geometry of each of MAST FI diagnostics. The flux surfaces are superimposed as dashed lines; the solid grey and black components, respectively, are cross-sections of poloidal field coils and graphite armour on the divertor and beam dumps. The green and grey shaded areas show the regions spanned by toroidally- and vertically-oriented SS beam-viewing FIDA lines of sight (LOS), respectively. The red and blue lines show examples of NC LOS, both midplane and diagonally-oriented chords. The tangency radius, denoted p, of one of these LOS is indicated. The coloured, curved lines show fusion proton/triton trajectories from the plasma which reach the CFPD. The NBI footprints are shown as red shaded regions; the two beams are denoted SS and SW. The cyan shaded area marks the region spanned by toroidal FIDA reference views, used for background subtraction. Also shown in (b) are the positions of the fission chamber (FC) and an outboard midplane Mirnov pick-up coil, used to detect MHD activity in the plasma. The midplane intersection radii of the active (SS beam-viewing) and reference (background subtraction) vertically-oriented FIDA chords are shown as dark brown lines in (b). Adapted from doi:10.1088/0741-3335/57/1/014006. © IOP Publishing. Reproduced by permission of IOP Publishing. All rights reserved.

investigation. MAST discharges typically lasted between 0.3 s and 0.6 s, with the plasma current ramp-up taking approximately 0.2 s. This is comparable with the timescale of current diffusion into the core of the plasma, hence the q-profile evolved throughout the current ramp and most of the flat-top phase of the discharge. The q-profile exhibited strongly reversed shear during the current ramp, indicating an off-axis peak in the current density profile, and tended to become monotonic late in the discharge.

The early part of MAST discharges was typically dominated by reversed-shear and toroidicity-induced Alfvén eigenmodes at frequencies of 50–150 kHz in the laboratory frame. Later in the discharge, lower-frequency fishbones (20–50 kHz) and eventually ideal-MHD kink modes at the toroidal rotation frequency of the bulk plasma (∼20 kHz) dominated the MHD activity. Spectrograms from the periods of interest in each of these scenarios are shown in figure 4. Shot #29207 *et sequation* included a period with a single neutral beam injecting 2.5 MW of power with a primary energy of 71 keV, throughout which chirping TAEs persisted, followed by a period with both neutral beams injecting a total of 3.5 MW of power with the primary energy of the second beam set at 61 keV. Large, quasi-periodic fishbones were observed during this phase. The second set of discharges, commencing with #29975, exhibited very strong fishbones occurring with semi-regular spacing between bursts; the TAEs are less distinct, and the early stages of the three discharges less similar to each other than those in the first set, so the analysis of this set focuses on the large fishbones occurring late in the discharge. The total NBI power in the second set was 3.0 MW, and the primary beam energies were 70 keV and 44 keV.

The evolution of the MHD activity is seen clearly in a time trace of a Mirnov pick-up coil signal. Figure 5 shows the raw data from the coil acquired during shot #29207. There is no clearly defined criterion to establish on the basis of the observed behaviour as to whether a given burst of MHD activity should be classed as a TAE, which is a normal mode of the background plasma, or an energetic-particle mode (EPM), the existence of which is dependent on the presence of an FI population. The classification indicated in figure 5 is based mainly on the frequency of the mode. The first set of weakly chirping MHD bursts is clustered close to the core TAE frequency. These modes are therefore identified as TAEs. The modes in the blue region in figure 5, seen in panel (b) of figure 4, exhibit much stronger frequency chirping and depart significantly from the TAE frequency. This suggests a strong energetic–particle drive which allows the modes to chirp down into the Alfvén continuum [15–17]. These modes exhibit highly variable spacing between bursts, and variable amplitude from one burst to the next. These are tentatively identified as TAEs with nonlinear coupling to EPM, although they will be referred to simply as 'chirping TAEs' hereafter. In the red region, although some of the features such as the temporal asymmetry of the TAE-EPM are still apparent in the first few bursts, the evolution of each burst is slower and more regular. The amplitude of successive bursts seems to follow a slowly evolving envelope, reaching a maximum at approximately 0.235 s, and there is much less inter-event variability. In accordance with the nomenclature used on other devices [18–21], these are called fishbones. A characteristic of the fishbones is that the frequency at the end of the burst coincides almost exactly with the core toroidal rotation frequency. These

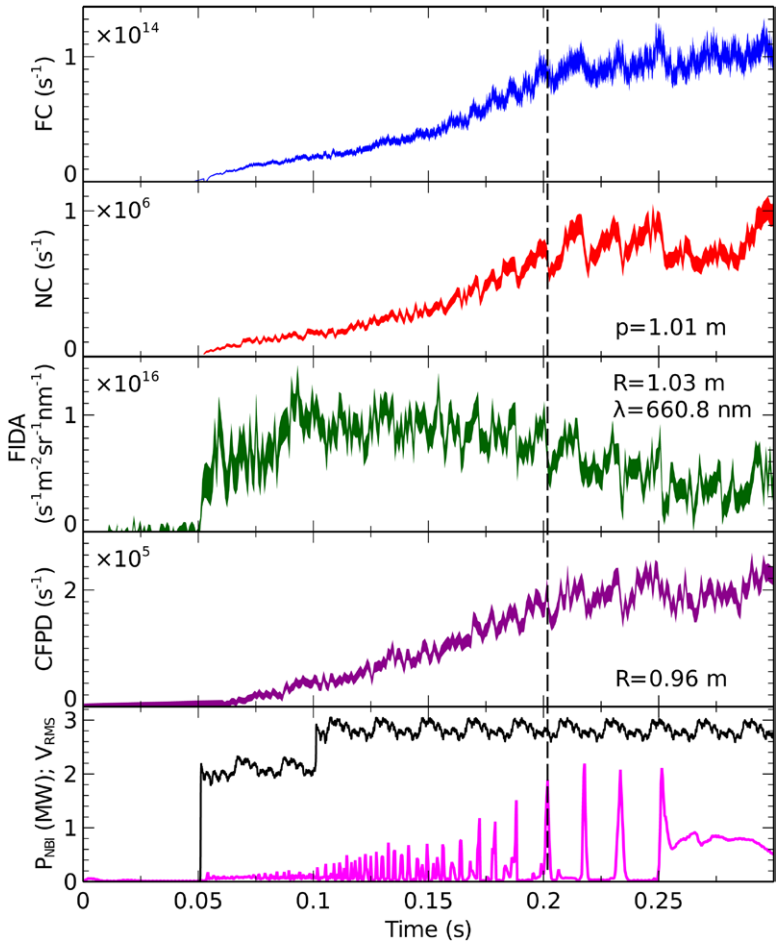

Figure 2. Time traces from single channels of the four MAST FI diagnostics, from shot #29980. The first four panels show, from top to bottom: fission chamber count rate; neutron camera count rate from a midplane chord with tangency radius p; FIDA spectral radiance at wavelength λ from a chord intersecting the axis of the SS neutral beam at major radius R; CFPD proton count rate from a channel with fusion proton trajectories intersecting the midplane at major radius R (where the values of p, R and λ are given by the labels in each panel). The thickness of the lines shows the statistical uncertainty in the data. Shown in the bottom panel is the total NBI power and the RMS voltage in a vertically-oriented Mirnov coil on the outboard midplane. The dashed vertical line marks the time at which a large fishbone occurred, with a corresponding reduction seen in each of the FI diagnostic signals.

are the chirping modes seen in panel (c) of figure 4. Finally, the steady-state internal kink, or *long-lived mode* (LLM), in MAST tended to persist from the end of the fishbone period until the end of the discharge.

The key parameters of the two sets of discharges studied in this work are summarised in table 1. We now examine the data acquired with the fission chamber, neutron camera and FIDA diagnostic during each set of discharges. A systematic analysis allows firm conclusions to be drawn regarding the effects of chirping modes on the FI population.

4. Effects of chirping modes on confined fast ions

4.1. Chirping TAEs

As shown in figure 6, a significant reduction in the NC count rate and FIDA radiance is observed to coincide with many TAE bursts in the first set of discharges. The timing of these drops in signal relative to the amplitude of the envelope of the Mirnov coil signal varies substantially between events. Not all drops in the diagnostic signals are associated with prominent chirping modes, neither are all bursts of magnetic activity correlated with significant changes in the diagnostic signals. In light of this variability, a quantitative approach must be adopted to determine the degree to which the reduction in FI confinement indicated by the NC and FIDA signals is correlated with chirping TAEs. No CFPD data are available for this set of discharges, since the diagnostic had not been installed at the time.

The first stage in identifying the correlation between TAE and FI diagnostic signals is to establish criteria for the identification of an 'event' in each case. Inspection of time traces such as those shown in figure 6 suggests that strong effects on the diagnostic signals are associated with TAE bursts with a large amplitude in the RMS Mirnov coil trace. Any increase in magnetic activity which exceeds a threshold RMS amplitude is therefore chosen to constitute an 'event' in the magnetics signal; this threshold is indicated by the dot-dashed horizontal lines in figure 6. In order to exclude drops in the NC and FIDA signals which occur due to statistical noise, or spurious drops in the net FIDA signal caused by rapid, transient spikes in background emission correlated with

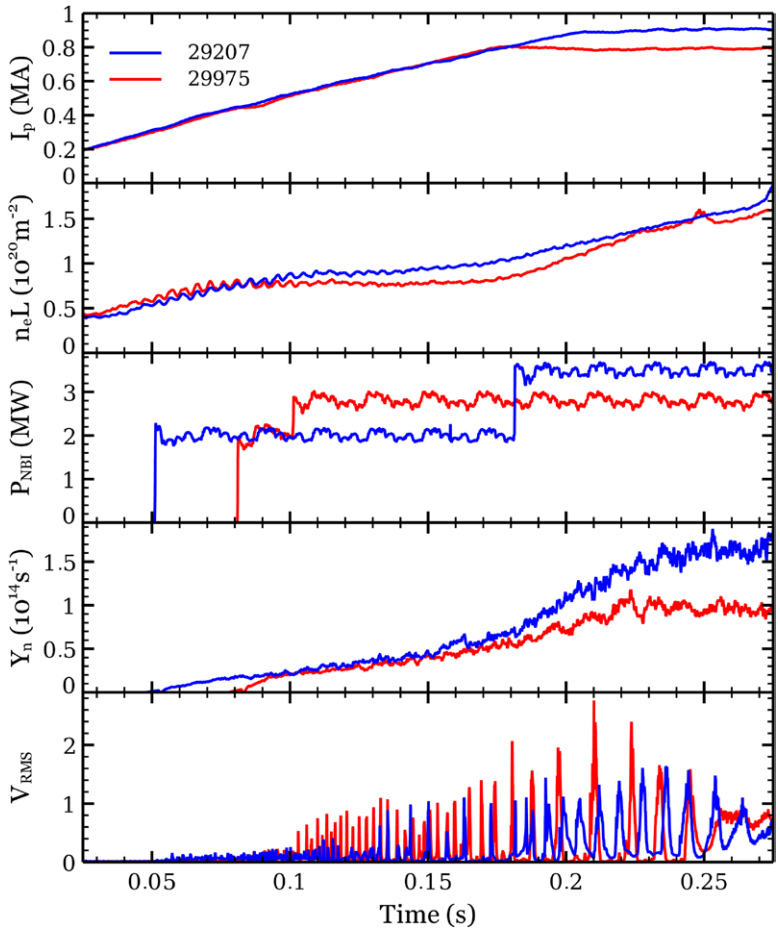

Figure 3. Global parameters of representative discharges from the two sets selected for analysis of the effects of TAEs and fishbones. The first set consists of shots #29207–#29210, and the second set includes shots #29975, #29976 and #29980. The panels show, from top to bottom: plasma current; line-integrated electron density measured with a CO_2 laser interferometer; total injected NBI power; global neutron rate measured with the fission chamber; and RMS amplitude of an outboard-midplane Mirnov coil signal sensitive to changes in the poloidal field.

TAE bursts, the condition imposed on these signals is that an 'event' constitutes a drop in signal which does not recover to the pre-event level within four time steps. With the integration time of the FIDA data set at 0.9 ms and that of the NC data set at 1.0 ms, this provides sufficient temporal resolution to allow each of the TAE bursts to be separated while ensuring that most of the 'events' represent true reductions in the part of the FI population to which the diagnostics are sensitive. Examples of qualifying events in the NC and FIDA signals are shown in figure 7. Note that a quadratic trend is removed from each of the time traces prior to analysis; this ensures that significant drops in diagnostic signals are not masked by the trend of the signal throughout the analysis period, which extends from 0.13 s–0.18 s in each of the four discharges analysed in this work.

Proceeding from the strict definition of an 'event' in the magnetics and FI diagnostic time traces, the criterion chosen to determine whether events coincide is that the onset time of the magnetics event must lie within a period extending from one time step before to two time steps after the start of the drop in FIDA or NC signal. This period is indicated by the shaded regions in figure 7. An asymmetric time window accounts for the fact that in many cases, it was observed that FI diagnostic signals started to decrease even when the amplitude of the MHD activity was still below the chosen threshold. By allowing some time for the magnetic coil signal to reach the threshold after the FI diagnostic signal has started to decrease, such events are captured by the identification process. The natural variation between events, arising due to the variable levels of drive and damping of the TAE, is thereby taken into account. For each FI diagnostic time trace, and for the analysis period during each discharge, an 'identification factor' may be defined to quantify the correlation between events in the diagnostic signals and the occurrence of TAE bursts. This factor is defined as

$$Q_{\mathrm{ID}} = \frac{\text{identified events}}{\text{total TAE events} + \text{false positives}}. \qquad (1)$$

Identified events are those events which exceed the threshold in the magnetic coil trace and are correctly identified as events by the FI diagnostic in question. *Total TAE events* are the number of above-threshold events in the magnetic coil signal. *False positives* are events which meet the identification criteria in the FI diagnostic signals, but during which the threshold in the magnetic coil signal is not exceeded. The top panel of figure 8 shows the results of the TAE identification

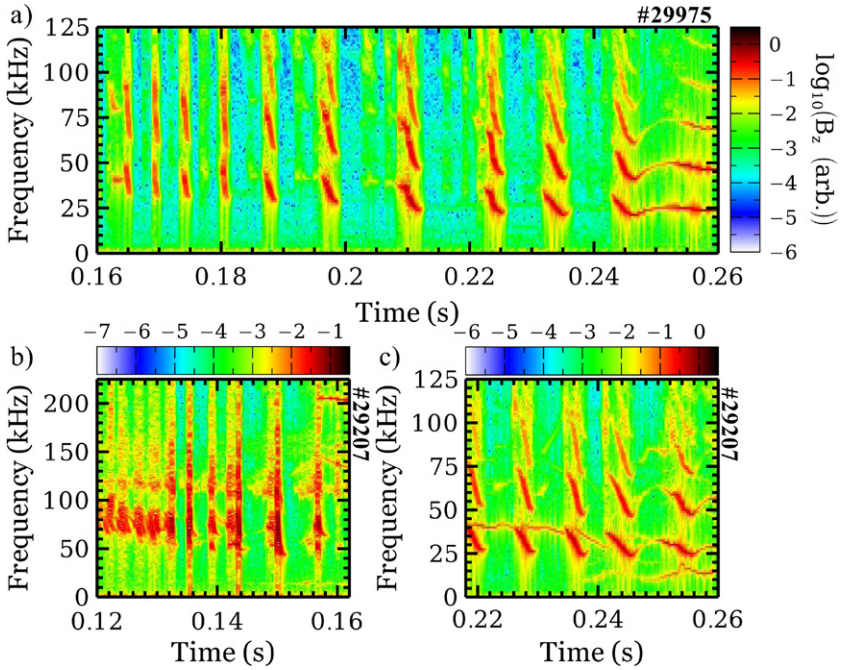

Figure 4. Spectrograms from an outboard-midplane Mirnov coil signal measuring the poloidal component of the perturbed magnetic field. (a) shows a period during shot #29975 in which chirping TAEs evolve into large-amplitude fishbones. (b) and (c) show two separate periods during shot #29207 in which chirping TAEs and large-amplitude fishbones, respectively, dominate the low-frequency magnetic activity. Note the extended vertical axis in (b) compared to (a) and (c). In neither of these shots are there any signs of high-frequency (compressional) Alfvén eigenmodes, which would appear at around 1 MHz; the absence of high-frequency MHD activity in the presence of low-frequency EPM is a characteristic feature of MAST plasmas.

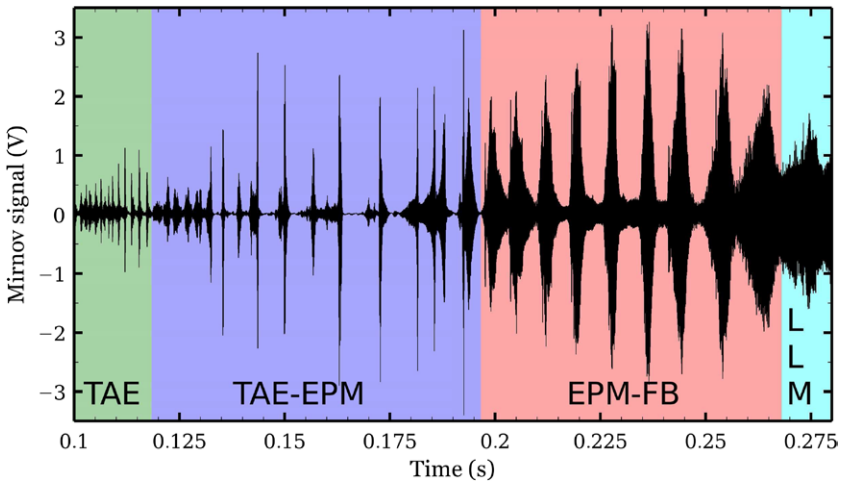

Figure 5. Time trace of the data acquired during shot #29207 by an outboard midplane magnetic pick-up coil. The coil is that used to generate the spectrograms in figure 4. The overlaid coloured regions show the qualitative classification of the different types of MHD activity. The classification is based on the temporal evolution of the frequency and amplitude of the signal. TAE = toroidal Alfvén eigenmode; EPM = energetic particle mode; FB = fishbone; LLM = long-lived mode, which is the name commonly given to the saturated internal kink mode in MAST.

analysis for all four discharges in this set. In each case, the FI diagnostics are best able to identify the effects of TAE bursts in the radial range where the signal is strongest; in the case of the NC this corresponds to the region close to the magnetic axis, and in the case of the FIDA diagnostic this corresponds to the mid-radius on the outboard side. This observation suggests that the limiting factor in the ability of the diagnostics to resolve the effects of chirping TAEs on FIs, at least in this set of discharges, is the SNR.

A meaningful assessment of the significance of these identification factors requires confidence intervals to be determined. The process adopted here was to randomly permute the data points in each FI diagnostic time series, and to establish an identification factor Q^*_{ID} based on the new, randomised time series. For each time series, the data were permuted 10 000 times to obtain 10 000 independent values of Q^*_{ID}. If the Q_{ID} of the original time series is greater than $n\%$ of these Q^*_{ID}, the probability of this value of Q_{ID} arising purely by chance is

Table 1. Parameters of the two sets of MAST discharges studied in this work.

	#29207+	#29975+
Flat-top plasma current (kA)	900	800
NBI power in TAE phase (MW)	2.0	3.0
NBI power in FB phase (MW)	3.5	3.0
Maximum beam voltage (kV)	71	70
Instabilities studied	TAE, FB	TAE

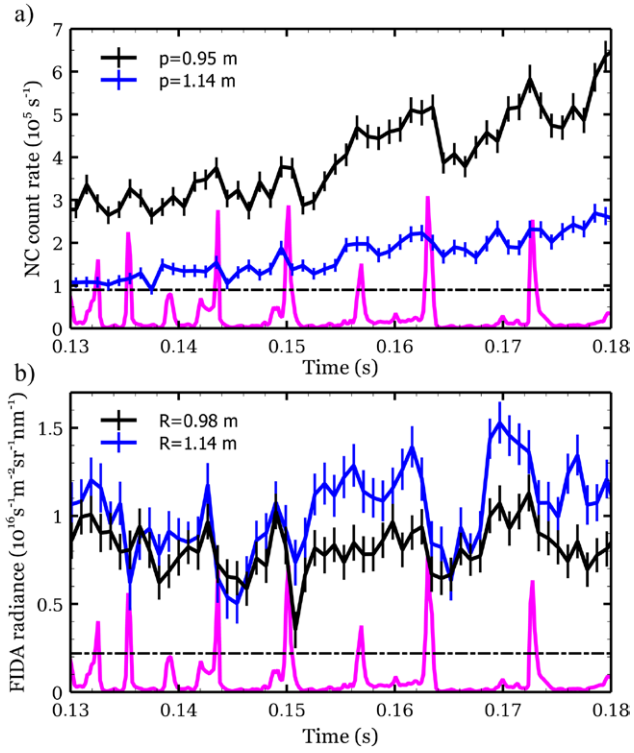

Figure 6. (a) Traces of NC count rates from the two midplane chords during a period in shot #29207 in which chirping TAE were active. The tangency radii of the two chords are labelled, and the magenta trace shows the RMS amplitude of an outboard-midplane Mirnov coil signal in arbitrary units. (b) Traces from two channels of the toroidally-viewing FIDA system during the same discharge, with the beam intersection radii labelled. Data are averaged over wavelengths 660.7 nm–661.3 nm, and therefore include FIDA emission from passing FI with energy $E > 46$ keV. Error bars on each trace represent random (statistical) uncertainty. In terms of the square-root of normalised poloidal flux, $s = \sqrt{\psi/\psi_a}$ where ψ_a is the poloidal flux enclosed at the plasma boundary, the positions of NC tangency/FIDA beam intersection radii are as follows: $p = 0.95$ m/$R = 0.98$ m $\leftrightarrow s \approx 0.1$; $p = 1.14$ m/$R = 1.14$ m $\leftrightarrow s \approx 0.5$.

less than $(100 - n)\%$. The dashed, horizontal lines in figure 8 mark the 90$^{\text{th}}$ percentile of 10 000 values of Q^*_{ID}, which is to say the 90% confidence level. The advantage of this procedure is that it is insensitive to the distribution of data points in the time series as long as the properties of this distribution are constant throughout the analysis period. To ensure that this was the case, the time series (with least-squares fitted quadratic trends removed) were subjected to the Dickey-Fuller test for the presence of unit root [22]. In all cases, the null hypothesis (that a unit root is present in the time series) was rejected at the 1% level, allowing the time series to be treated as stationary.

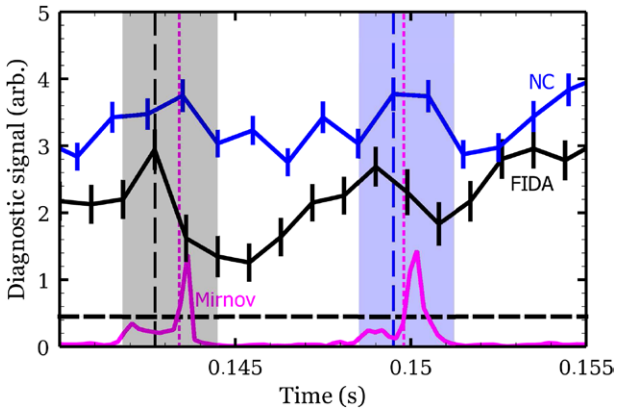

Figure 7. Drops in NC and FIDA signals which qualify as 'events' for the purposes of determining the correlation with chirping TAE. The dashed vertical black and blue lines mark the onset times of events in the FIDA and NC signals respectively. Dotted vertical magenta lines mark the onset times of events in the RMS Mirnov coil signal, in which the magenta trace exceeds the threshold shown by the dashed horizontal line. The shaded regions which extend from one time step before to two time steps after the events in FI diagnostic signals indicate the period within which the magnetics event must occur in order to be counted towards successful identification; clearly both of the events highlighted here satisfy this criterion. The NC trace plotted here with a quadratic trend removed corresponds to that plotted in black ($p = 0.95$ m) in figure 6. The FIDA trace shown here with a quadratic trend removed was plotted in blue in figure 6 ($R = 1.14$ m).

In the top panel of figure 8, the majority of data points lie on or above the relevant dashed line marking the 90% confidence level. If there were no correlation between FI diagnostic signals and TAE bursts, only one point in ten would be expected to lie on or above this confidence level. It can therefore be said with confidence that a significant reduction in the confined FI density in these plasmas is correlated with chirping TAEs.

4.2. Fishbones

Each of the discharges in the set analysed above also exhibited well-spaced, quasi-periodic fishbones, as seen in panel (c) of figure 4. The method described in the previous section was applied to the NC and FIDA signals to establish the correlation between these signals and the fishbones. In this analysis, the threshold applied to the RMS Mirnov coil signal was increased to account for the larger amplitude of the fishbone bursts compared to the TAE bursts. The dashed, horizontal lines in each panel of figure 9 indicate the chosen threshold. The width of the time window which was searched for a burst in Mirnov coil signal corresponding to each drop in NC or FIDA signal was also widened compared to that used in the TAE analysis. This widening accounts for the fact that the fishbones evolve more slowly than the TAEs and therefore take longer to have a significant effect on the FI population. The window was extended by half a time step in each direction, thus covering the period from 1.5 time steps before to 2.5 time steps after the commencement of the drop in FI diagnostic signal. Significant drops in NC and FIDA signals

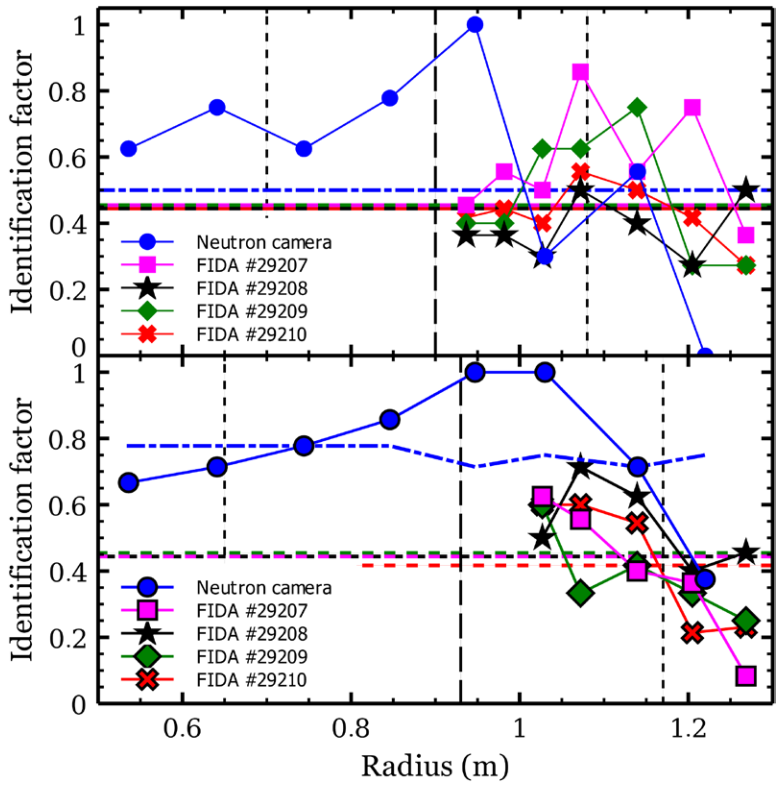

Figure 8. Top panel: TAE identification factors, defined according to equation (1), for the NC and FIDA diagnostics during the period 0.13 s–0.18 s in shots #29207–#29210. The vertical dashed and dotted lines mark the approximate positions of the magnetic axis and minimum safety factor ($q_{\min}$) surfaces, respectively. The dashed horizontal lines of various colours mark the 90% confidence level for event identification in the corresponding FI diagnostic signal; data points have less than a 10% chance of lying above these lines assuming random time series. Bottom panel: as above but for fishbones occurring in the period 0.208 s–0.258 s during the same set of discharges. The two innermost FIDA channels are excluded from this panel due to the contamination of the spectra by SW beam emission.

are clearly seen to accompany the fishbone bursts in figure 9. The results of the analysis described above are shown in the bottom panel of figure 8. As in the case of the TAEs, both diagnostics see significant drops in signal correlated with the fishbones. In many of the channels the confidence in the correlation exceeds 90%. Note that the two innermost channels of the FIDA system cannot be included in this analysis since the spectra are strongly contaminated with SW beam emission.

In previous studies of MAST FIDA data [23], it was found that the relative change in the core FIDA signal due to the fishbones correlated strongly with the maximum RMS amplitude of the Mirnov coil signal and only weakly with the amplitude of the perturbation. This analysis was repeated for the data from the recent set of discharges (#29207 *et sequation*). Figure 10 shows the scaling of the drops in FIDA signal with the amplitude of the fishbones and with the RMS amplitude of the perturbation in the Mirnov coil signal. The wavelength used in figure 10 corresponds to a minimum FI energy of 46 keV. The data are averaged over three channels with beam intersection radii 1.03 m, 1.07 m and 1.14 m. A different symbol is used for each shot, but the regression analysis takes into account the whole data set. As in the earlier study [23], the drops in FIDA signal are correlated much more strongly with the RMS Mirnov coil signal than with the fishbone amplitude. The correlation coefficient r is not particularly high in either case, but given the sizes of the error bars the probability of the value of χ^2 being greater than or equal to the observed value, given that a linear relationship exists, is 0.330 in the case of the correlation with the RMS Mirnov coil signal. For the correlation with the fisbone amplitude, this probability is 0.154. The possibility of a correlation with the RMS pick-up coil signal is therefore not excluded nearly as strongly as the possibility of a correlation with the fishbone amplitude.

A similar linear scaling was found between the drops in global neutron rate and the peak Mirnov coil signal in a previous study of MAST data [24]. This suggests that the strength of the interaction between the fishbones and the FIs is sensitive to the frequency of the perturbation as well as to its amplitude, since $\dot{B}_\theta \approx \omega \tilde{B}_\theta$. Here, $\dot{B}_\theta$ is the time derivative of the poloidal magnetic field, to which the Mirnov coil signal is proportional assuming a fixed mode location, and ω and $\tilde{B}_\theta$ are the frequency and amplitude of the mode. Such a relationship was previously found between drops in the global neutron rate and $\langle \dot{B}_\theta \rangle_{\mathrm{RMS}}$ during TAE bursts in DIII-D [25], while no linear dependence on $\langle \dot{B}_\theta \rangle_{\mathrm{RMS}}$ was seen in the case of fishbone bursts. A linear correlation was later found, albeit in a smaller data set, between drops in the neutron rate and the amplitude $\tilde{B}_\theta$ of chirping modes in the fishbone-EPM frequency range [26]. In NSTX meanwhile, a very weak linear scaling was identified between FI losses and mode amplitude $\tilde{B}_\theta$ in the case of both EPMs and TAEs, with TAEs having a stronger effect for a given mode amplitude [27]. Fishbones were not included in that data set, and the correlation with $\dot{B}_\theta$ was not examined. For the changes

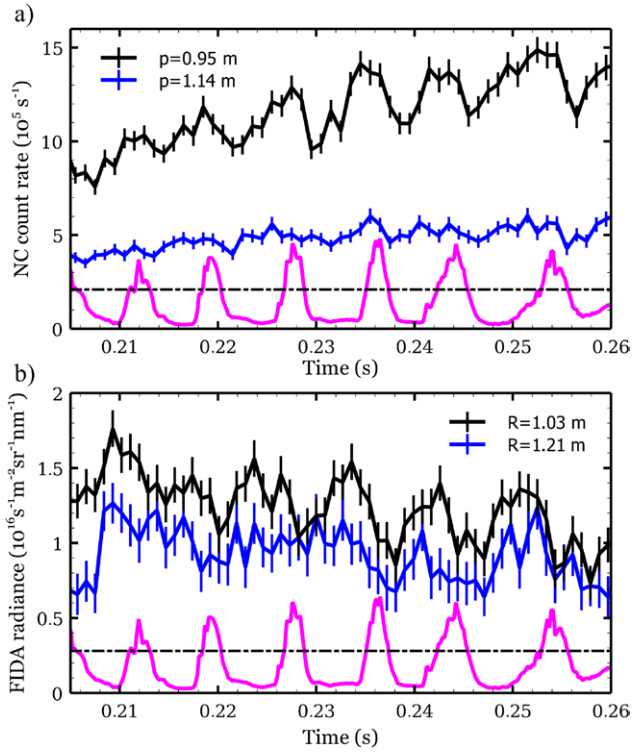

Figure 9. (a) Traces of NC count rates from the two midplane chords during a period in shot #29207 in which fishbones were active. The tangency radii of the two chords are labelled, and the magenta trace shows the RMS amplitude of an outboard-midplane Mirnov coil signal in arbitrary units. (b) Traces from two channels of the toroidally-viewing FIDA system during the same discharge, with the beam intersection radii labelled. Data are averaged over wavelengths 660.7 nm–661.3 nm, and therefore include FIDA emission from passing FI with energy $E > 46$ keV. Error bars on each trace represent random (statistical) uncertainty. In terms of normalised poloidal flux as defined in the caption of figure 6, the NC tangency radii are at $s \approx 0.05/0.45$ for $p = 0.95$ m/1.14 m. FIDA beam intersection radii are at $s \approx 0.20/0.60$ for $R = 1.03$ m/1.21 m.

in the FIDA signal associated with the chirping TAEs discussed in the previous section, no meaningful correlation was found with either $\langle \dot{B}_\theta \rangle_{\mathrm{RMS}}$ or with $\tilde{B}_\theta$. The present result therefore raises the question of which quantity is the better proxy for the ability of chirping modes to redistribute FIs, particularly in the presence of mixed low and high-frequency modes.

Since the tangency radius of the NC was scanned between discharges in this set, the correlation analysis presented in figure 10 unfortunately cannot be extended to this diagnostic. Furthermore, the drops in the global neutron rate due to these fishbones are small and difficult to distinguish from noise or from perturbations caused by changes in bulk plasma parameters or non-resonant MHD modes. We therefore move on to the consideration of the possibility that as well as causing real-space or velocity-space transport of resonant FIs as suggested by the results in this section, the TAEs and fishbones may also cause losses of FIs from the plasma.

4.3. Fast-ion losses due to resonant MHD instabilities

Spikes in the D_α radiation from the edge of the plasma and from the divertor are observed to coincide with many chirping modes. Figures 11 and 12 show examples of this behaviour from shot #29207. Bursts in the Mirnov coil trace coincide with a significant reduction in FIDA and neutron emission from the core of the plasma, as well as with pronounced spikes in the signal from a filtered D_α monitor viewing the edge of the plasma close to the midplane. These spikes in D_α light were hypothesised to be the result of CX reactions between FIs ejected from the plasma by the modes, and neutrals close to the plasma boundary. The open divertor in MAST meant that deuterium recycled from the plasma at the divertor plates was able to circulate freely in the vacuum vessel, forming a dense 'blanket' of neutrals at the edge of the plasma.

To test this hypothesis regarding the origin of the D_α spikes, the *passive FIDA* emission provides useful information. Passive FIDA is the D_α light emitted by reneutralised FI which have undergone CX with edge neutrals rather than with beam or halo neutrals. By inspecting the time trace of passive FIDA during a time window in which edge D_α spikes are observed, the mechanism giving rise to these spikes is firmly established to be related to the FIs. The bottom panels of figures 11 and 12 show time traces of passive FIDA from a reference channel ($R = 1.33$ m) during the period in which large-amplitude TAEs or fishbones and D_α spikes are observed. Each trace corresponds to a particular wavelength of FIDA radiation. E_{min} is the minimum energy of a reneutralised ion, which could give rise to D_α emission at the observed wavelength. The signal at each wavelength therefore consists of two components: a FIDA component from reneutralised FIs with $E \geqslant E_{\mathrm{min}}$; and a bremsstrahlung component which is approximately equal for all wavelengths in this range. The spikes in passive FIDA emission are clearly seen to be suppressed close to the beam injection energy, which is 71 keV during this shot. This observation demonstrates conclusively that the D_α spikes are at least partially caused by reneutralised FIs rather than by thermal neutrals or perturbations to bremsstrahlung radiation. This implies that both TAEs and fishbones caused losses of FIs from these plasmas.

Analysis and interpretation of the FIDA and NC observations reveals that both TAEs and fishbones cause FIs to be transported from the core of the plasma and even lost through the plasma boundary. The next step in this analysis is to attempt to model the effects of the modes on FIs using the *ad hoc* models available within TRANSP.

5. TRANSP modelling of fast-ion redistribution

5.1. Anomalous transport models

Two mechanisms are available within NUBEAM to allow the effects of TAEs and fishbones on the FIs to be modelled. The redistribution may be modelled as a combination of diffusive and convective transport, with user-specified diffusion and advection coefficients specified as a function of radial position, time and energy. Without first-principles modelling of the underlying physics to guide the choices of these coefficients, however, only the simplest models are practically applicable. In the modelling described in this section, anomalous diffusion was varied as a function of time but was taken to be

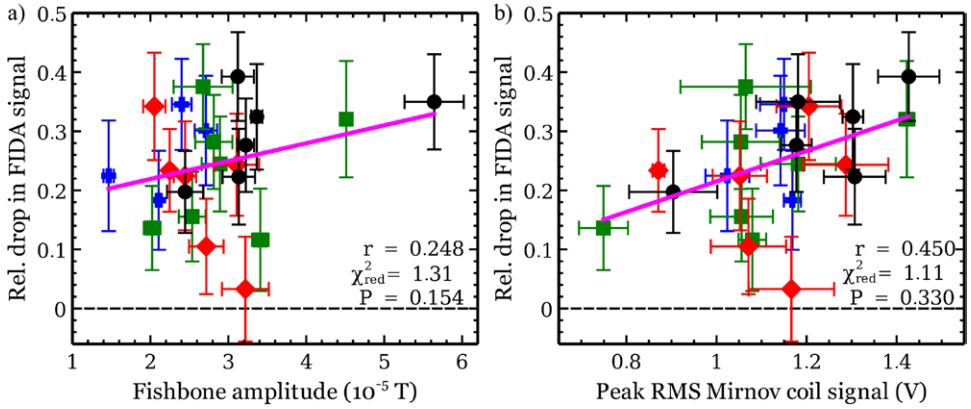

Figure 10. Relative change in FIDA signal plotted against (a) the amplitude of the fishbone perturbation and (b) the maximum RMS amplitude of the Mirnov coil signal for a set of 23 fishbones in shots #29207–#29210. Each data point corresponds to a single fishbone, and different symbols are used for each discharge. The relative drop in signal is defined as $(S_i - S_f)/S_i$ where S_i and S_f are the maximum and minimum signal before and after each fishbone respectively, The correlation coefficient r, reduced χ^2 and cumulative chi-square probability $P = \Pr(X^2 \geqslant \chi^2)$ are shown in each panel. Data are averaged over $R = 1.03$ m–1.14 m at $\lambda = 660.7$ nm. Error bars are derived from the statistical uncertainty in the FIDA signal, and from the standard deviation of three data points near the maximum of the smoothed RMS Mirnov coil signal.

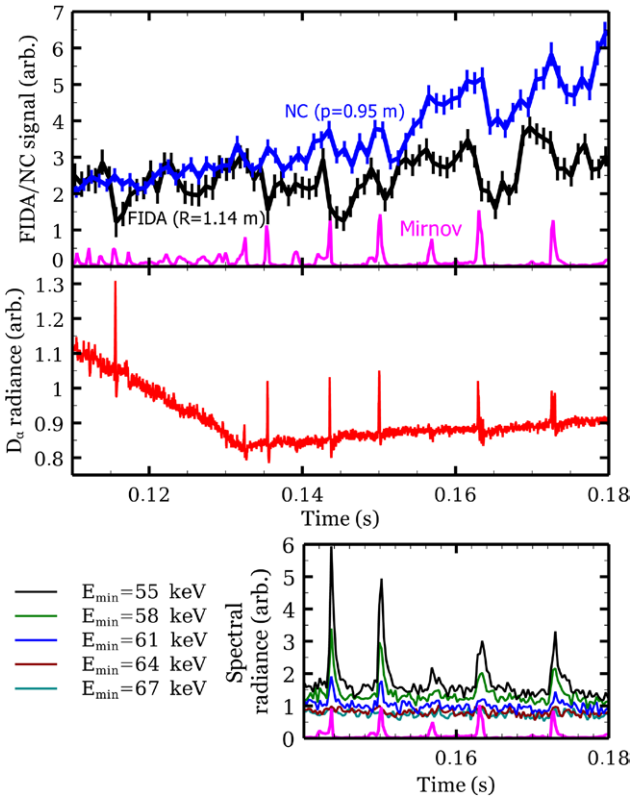

Figure 11. Chirping TAEs during shot #29207 are observed to cause large drops in core NC and FIDA signals which in most cases take several milliseconds to recover to the pre-event level (top panel). Coincident with the largest of these bursts, spikes in D_α radiation from the edge of the plasma are observed (middle panel). A large drop in FIDA signal and a spike in edge D_α are also observed at around 0.115 s, despite the fact that only a small TAE, and no drop in NC signal, is observed at this time. The nature of this event is unknown, but the observations suggest a spatially-localised loss of FIs. The bottom-right panel shows the signal from a background-viewing FIDA channel at wavelengths corresponding to minimum detectable FI energies E_{min} close to the beam injection energy, which was 71 keV. This signal comprises bremsstrahlung and passive FIDA emission, as discussed in the text. The midplane intersection radius of the LOS from which these data are obtained is $R = 1.33$ m.

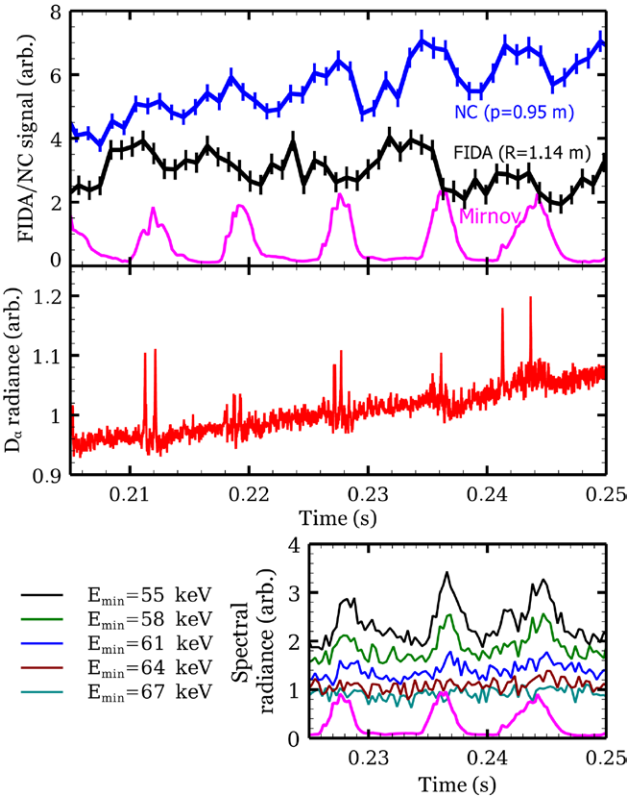

Figure 12. Fishbones during shot #29207 are observed to cause large drops in core NC and FIDA signals which in most cases take several milliseconds to recover to the pre-event level (top panel). Coincident with these bursts, spikes in D_α radiation from the edge of the plasma are observed (bottom panel). The D_α spikes in this case exhibit more structure, last longer, but have a smaller amplitude than in the case of the TAEs. As in the previous figure, the bottom-right panel shows background emission (bremsstrahlung and passive FIDA) at wavelengths corresponding to minimum detectable FI energies E_{min} close to the beam injection energy.

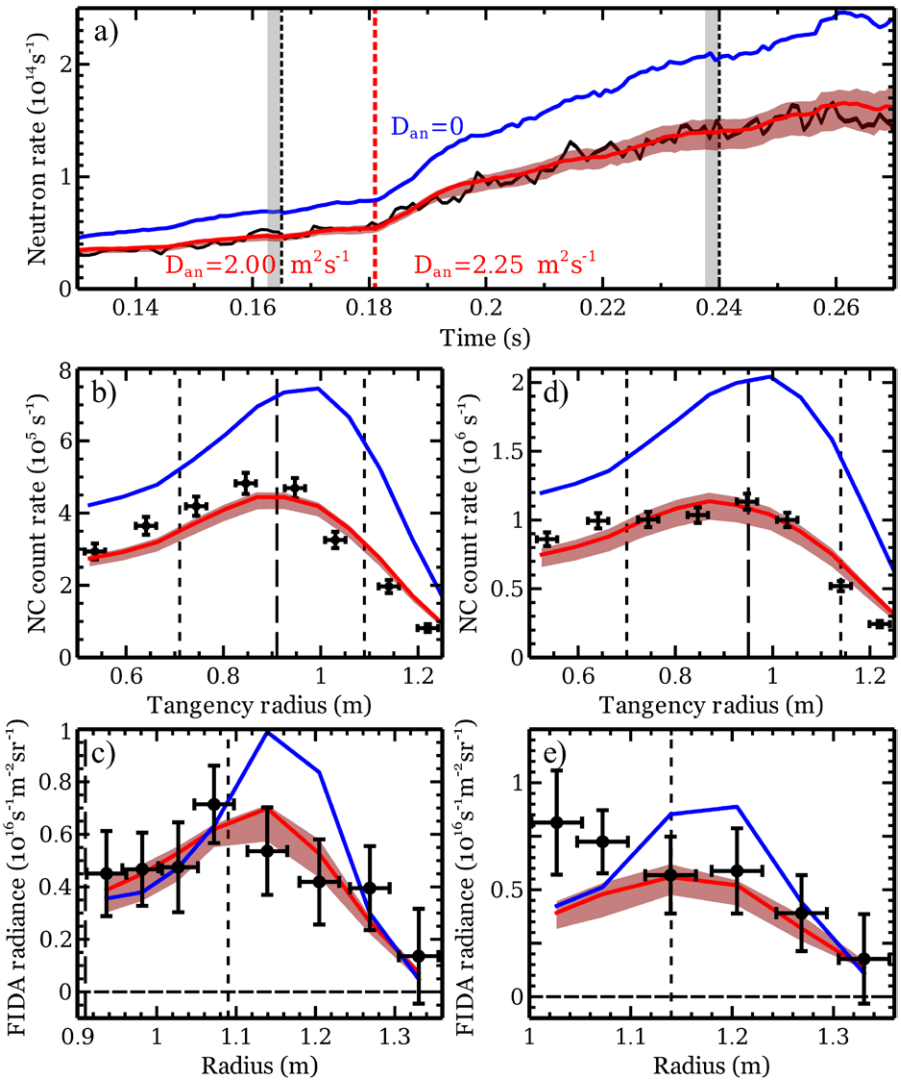

Figure 13. Comparisons between measured and NUBEAM-modelled FI diagnostic time traces and radial profiles in the presence of chirping TAEs and fishbones. Panel (a) shows the global neutron rate measured in shot #29210 (black) compared to that modelled with (red) and without (blue) spatially-uniform anomalous FI diffusion in TRANSP. The values of anomalous diffusivity used in these simulations are given in the labels. The forward-modelled NC and FIDA profiles are compared to the measured profiles in panels (b) and (c) for $t = 0.165$ s and in panels (d) and (e) for $t = 0.240$ s. Contamination of the core FIDA signal with SW beam emission at the later time means that the two channels between 0.9 m and 1.0 m cannot be included, and the signal in the two channels between 1.0 m and 1.1 m is artificially elevated. The vertical dashed and dotted lines in panels (b)–(e) indicate the approximate radial positions of the magnetic axis and minimum-q surfaces. $\lambda = [660.9 - 661.9]$ nm for FIDA data.

radially uniform throughout the plasma. Convective transport was not applied, since diffusive transport was found to reproduce the observations reasonably well. The effect of diffusion is to cause radial transport of FIs at a rate proportional to the radial gradient of the FI density. The resulting flux is

$$\Gamma_{\mathrm{FI}} = -D_{\mathrm{an}} \nabla_r n_{\mathrm{FI}},$$

where D_{an} is the spatially and temporally-varying anomalous FI diffusivity. The diffusive model was previously applied successfully to model the global neutron rate and NC count rate profiles in MAST discharges with on and off-axis NBI [24].

The second FI transport mechanism available within NUBEAM is an *ad hoc* fishbone loss model. This model takes as input parameters: the time of the first fishbone and the time at which the model is switched off; the duration of the fishbone burst and the characteristic loss time of the FIs while the fishbone is active; the time between fishbone bursts; and the minimum and maximum values of energy and pitch of the affected FIs. This model was successfully used to reproduce global and local neutron emission from MAST plasmas as described by Klimek *et al* [28]. In the present work, however, FIDA observations are used as an additional constraint on the parameters of the model.

In the following sections the results of TRANSP modelling using anomalous diffusion and the fishbone model are presented.

5.2. Modelling with anomalous diffusion

The series of discharges #29207 *et sequation*, with chirping TAEs and quasi-periodic fishbones, provided an opportunity to test the diffusive NUBEAM modelling in the presence of resonant MHD activity. Time slices averaged over 3 ms, from 0.162 s–0.165 s during the chirping TAE phase and from

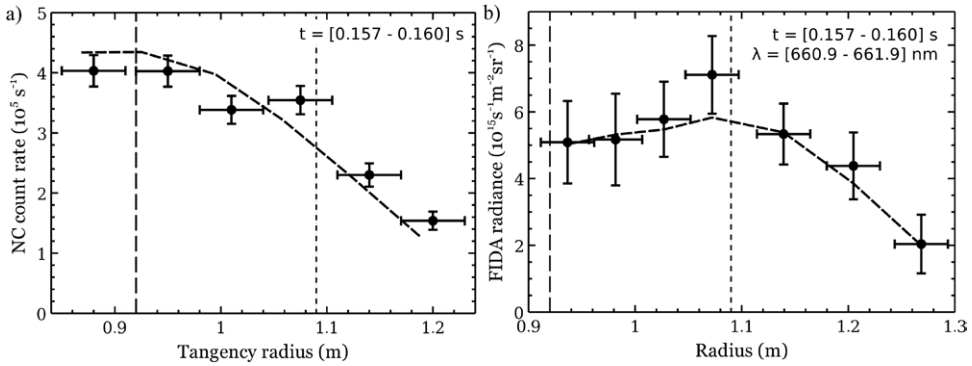

Figure 14. Profiles of measured and modelled NC and FIDA signals averaged over the period 0.157 s–0.160 s during shot #29976 (with the measured NC profile including data from similar discharges #29975 and #29980). The modelled profile is based on a simulation with an anomalous diffusivity of 3.0 m^2.s^{-1} at this time during the discharge. The vertical dashed and dotted lines mark the approximate radial positions of the magnetic axis and minimum-q surface.

0.237 s–0.240 s during the fishbone phase, were used for a comparison between NUBEAM modelling and FI diagnostic signals under the assumption of spatially-uniform anomalous diffusion. The results of this comparison are shown in figure 13. The shading around the red curves in this figure represents the uncertainty introduced into the modelling by the uncertainty in various plasma parameters. Electron temperature and density and effective plasma charge were varied within the limits of the experimental errors in order to derive these model uncertainties.

Clearly the introduction of anomalous diffusion is sufficient in this case to model the effects of both chirping TAEs and fishbones on the FI distribution, at least to the extent that the distribution may be constrained by the available diagnostics. The values of anomalous diffusivity used here are moreover very similar to those employed in previous studies of the effects of Alfvén eigenmodes on FI confinement [29]. It is worth noting that at the two times shown in figure 13 the measured profiles are averaged over periods during which a significant MHD perturbation occurred; profiles during selected MHD-quiescent windows shortly before a TAE or fishbone burst exhibit increased signal levels, although the signal still does not reach the level modelled in the absence of anomalous FI diffusion. The coarse assumption of spatially-uniform diffusivity, held constant over a long period, cannot capture the dynamics of individual bursts of MHD and the interaction of these bursts with the FIs.

5.3. Inclusion of the fishbone model

Figure 14 shows that spatially-uniform anomalous diffusion models well the early part of shot #29975 *et sequation* during which chirping TAEs were active. The forward-modelled NC and FIDA profiles show good agreement with the measured profiles at $t = 0.160$ s, when a diffusivity of $D_{\rm an} = 3.0$ m^2.s^{-1} allows the TRANSP modelling to match the measured global neutron rate to within 10%.

Later in each of the discharges from this set, a series of large fishbones caused transient FI redistribution, which the simple diffusive transport model is unable to capture. This redistribution resulted in drops of ∼10% in the global neutron rate, as seen in figure 15. No significant changes in profiles of electron density or temperature are associated with these fishbones, so

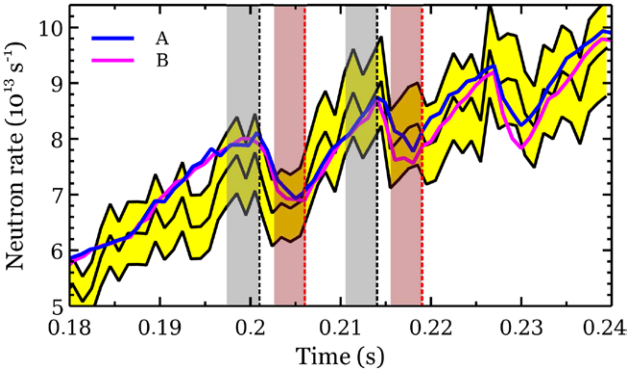

Figure 15. A comparison between the measured (black trace, with yellow shaded region indicating statistical uncertainty) and modelled (blue and magenta traces) global neutron rates for shot #29976 with the fishbone model applied within NUBEAM. The fishbones were specified to occur from 0.201 s to 0.230 s with a period of 12.8 ms and a duration of 4 ms. The grey and red shaded rectangles indicate the periods before and after the first two fishbones, over which synthetic FI distributions and measured NC and FIDA signals were averaged to produce the subsequent figures in this section.

changes in the beam-ion deposition cannot account for the observed reduction in neutron rate or FIDA signal.

As mentioned earlier, NUBEAM contains a fishbone model which allows FIs to be expelled from the plasma within a specified part of velocity space, with a chosen periodicity and characteristic loss time. This model was previously used to reproduce changes in global and local neutron emission in another series of MAST discharges [28], but the FIDA data were unavailable for those shots. In the series of discharges studied here, the fishbone model was initially used with settings similar to those applied in the previous study, cutting out all FIs with $E \geqslant 50$ keV and with $-0.5 \leqslant p \leqslant 0.5$. It was found, however, that despite the relatively successful match to the global neutron rate and the changes in the NC count rate profiles achieved using this model, the changes in the FIDA signal were not reproduced. The toroidal FIDA views are insensitive to ions with such a small ratio of parallel to perpendicular velocity, since the LOS are almost tangential to the magnetic field at the point of beam intersection in the core of the plasma. If only those ions with $-0.5 \leqslant p \leqslant 0.5$ were affected by the fishbones, the FIDA signal

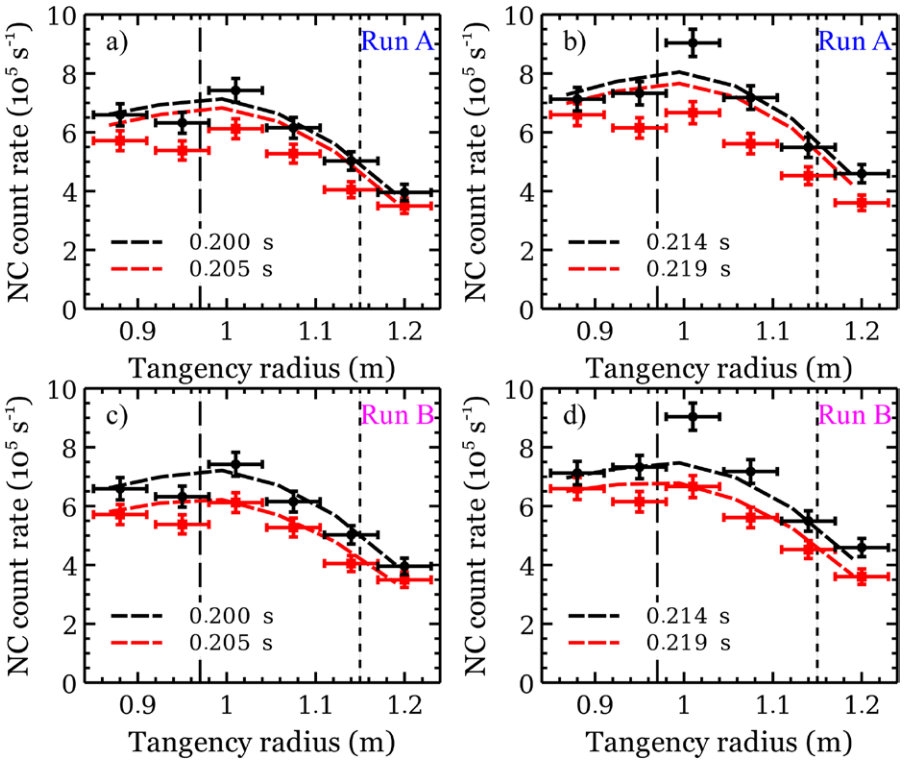

Figure 16. Profiles of the NC count rate before (black points) and after (red points) the first two fishbones in shots #29975, #29976 and #29980. Panels (a) and (b) compare the measured profiles to those forward-modelled from the neutron emission profiles generated in TRANSP run A for shot #29976 (dashed lines), while panels (c) and (d) show a comparison with TRANSP run B for the same shot. The vertical dashed and dotted lines mark the radial positions of the magnetic axis and minimum-q surface.

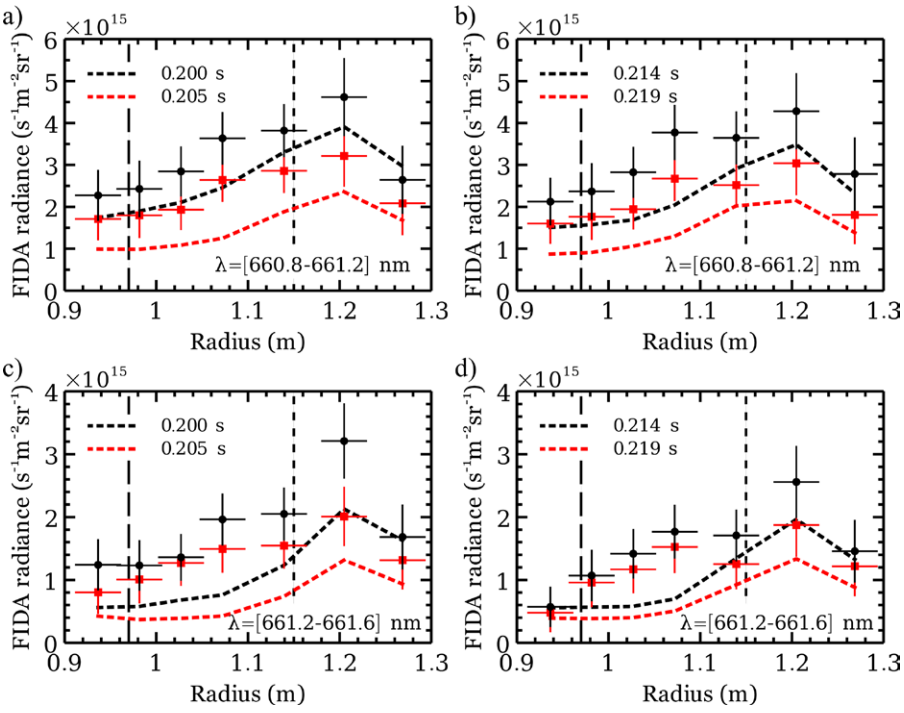

Figure 17. Profiles of FIDA radiance before (black points) and after (red points) the first two fishbones in shot #29976. Panels (a) and (b) compare the measured profiles to those forward-modelled with FIDASIM from the FI distributions generated in TRANSP run A, in a wavelength range corresponding to a minimum FI energy of 48 keV (dashed lines). Panels (c) and (d) show a comparison at higher wavelengths, with $E_{\mathrm{min}} = 57$ keV. The vertical dashed and dotted lines mark the radial positions of the magnetic axis and minimum-q surface.

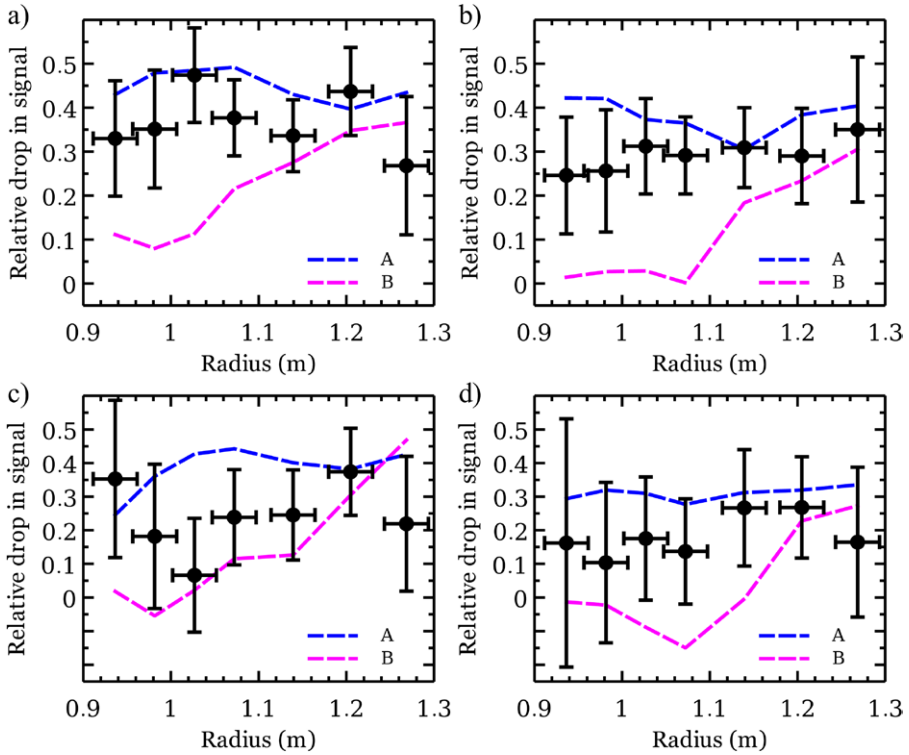

Figure 18. Profiles of the relative reduction in FIDA radiance, defined as $(S_i - S_f)/S_i$, where S_i and S_f are the pre- and post-fishbone signals, caused by two fishbones in shot #29976. The measured relative changes are compared to those derived from the FIDAsim profiles based on Transp run A (blue dashed lines) and B (magenta dashed lines). The wavelengths are the same as those in the corresponding panels of figure 17; panels (a) and (c) correspond to the first of the modelled fishbones, while (b) and (d) correspond to the second fishbone.

would not change. By contrast, the large fishbones in these shots are observed to cause significant drops in FIDA signal at all radii from the magnetic axis to the plasma boundary. This observation informed the choice of energy and pitch boundaries in the fishbone model within which the FIs were removed. An iterative process was adopted by which the simulation parameters were at first coarsely modified to converge on the global neutron rate, then modified more precisely to converge on the relative changes in either the FIDA radial profiles (run 'A') or in the NC radial profiles (run 'B'). The neutron rate comparisons from the two most successful simulation runs are shown in figure 15. The characteristic loss time of the affected FIs was 3 ms in run A and 1 ms in run B. In run A, FIs with $50\ \text{keV} \leqslant E \leqslant 75\ \text{keV}$ and $0.69 \leqslant p \leqslant 0.93$ (evaluated at either of the two previous midplane crossings) were removed by the fishbones; these values of pitch correspond to co-passing FIs. In run B, these ranges were $60\ \text{keV} \leqslant E \leqslant 70\ \text{keV}$ and $0 \leqslant p \leqslant 0.7$, corresponding to trapped and co-passing FIs. In addition to the fishbone model, a small anomalous diffusivity of 0.15 $\text{m}^2.\text{s}^{-1}$ was applied to FIs with $E \leqslant 45$ keV during the fishbone phase in both simulations; D_{an} decreased linearly with energy from 0.150 $\text{m}^2.\text{s}^{-1}$–0.105 $\text{m}^2.\text{s}^{-1}$ between 45 keV and 75 keV.

Figure 16 shows that Transp run B, in which high-energy FIs with $0 \leqslant p \leqslant 0.7$ are removed by the fishbones, produces a good match to the relative size of the observed changes in the NC signal across the plasma radius as well as to the shape of the NC profile. Run A produces a similar match to the profile shape, but significantly underestimates the size of the drops in signal due to the fishbones.

The same pair of Transp runs was used to generate synthetic FIDA profiles. Although the absolute match between the modelled and measured signal levels was slightly better for run B, the simulated fishbones with these settings failed to cause the observed reduction in the core FIDA signal. Figure 17 shows that run A, by contrast, matches the relative change in signal fairly well and also matches the profile shape well, at least at mid-high energies (top panels), even though it underestimates the magnitude of the signal. The comparison between the two runs in terms of their match to the relative change in FIDA signal is quantified in figure 18. This contains the same data as figure 17, but with the absolute signal level factored out. The relative change in modelled FIDA signal due to the fishbones in Transp run B is also shown in this figure. Clearly the removal of high-energy passing ions, as performed in run A, reproduces the FIDA observations better than the alternative model. The resonant interaction of passing FIs with fishbones finds a precedent in results from the PBX tokamak [30], and was explained theoretically by Betti and Freidberg [31].

The fact that run A systematically slightly overestimates the magnitude of the changes in FIDA signal across the plasma radius, while run B underestimates these changes in the core but matches them well at the edge, suggests that the real effect of the fishbones is best represented by a combination of these models. It is reasonable to suppose that the properties which allow FIs to resonate with the mode, and hence to be strongly redistributed, are a function of radial position in the plasma. This dependence cannot be captured with the simple *ad hoc*

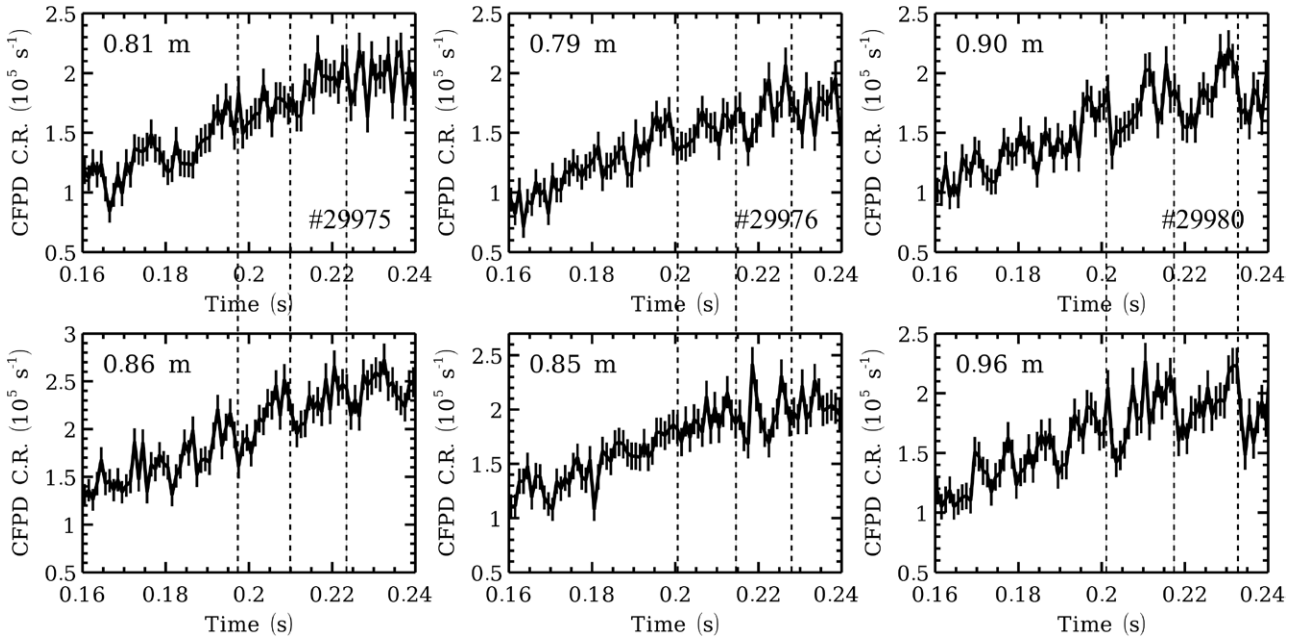

Figure 19. Time traces of data from two channels of the CFPD during the large fishbones in shot #29975 *et seq.*. Each column includes data from a single shot, with the dotted vertical lines marking the time at which the amplitude of each of the three largest fishbones reached a maximum. The label in each panel indicates the midplane intersection radius of the centre of the bundle of fusion proton trajectories which reaches the detector. The magnetic axis is located at approximately $R = 0.97$ m.

model available in NUBEAM. More realistic simulations must await the inclusion of a first-principles model of resonant transport in the global transport simulations. This would allow the affected range of pitch, for example, to be varied smoothly between two rather different sets of parameters used in the present work.

In the set of shots commencing with #29975, the radial position of the CFPD was scanned between discharges. This allowed the effects of the large fishbones on the CFPD count rate to be determined as a function of the midplane intersection radius; the data from each channel are shown in figure 19. It is apparent that the strongest effect of the fishbones on the count rate is observed on trajectories intersecting the midplane close to the magnetic axis. Channels with midplane intersection radii from 0.86 m to 0.96 m see a strong depletion in the count rate coinciding with each of the large fishbones, while those at 0.79 m and 0.81 m see only a weak effect. Without a reliable synthetic diagnostic, the fishbone modelling carried out with TRANSP/NUBEAM cannot be validated against these measurements. Nonetheless, the observation of fishbone-induced drops in signal in *all* of the traces in figure 19 is broadly consistent with the NC and FIDA measurements, which show a significant reduction in signal across the core of the plasma.

6. Summary and conclusions

Resonant energetic-particle-driven MHD instabilities observed in the MAST include chirping TAEs and fishbones. In this work, observations of changes in the FI diagnostic signals correlated with each of these instabilities were presented and the interpretation of these observations was discussed. The results of TRANSP modelling in which anomalous FI transport or loss processes were invoked to try to match the observations were presented and compared with the measurements. Four main conclusions are supported by the results presented here:

- Drops in both FIDA and NC signals are correlated with chirping TAE and fishbones at a statistically significant level, indicating a reduction in the confined FI density.
- Chirping TAEs and fishbones cause enhanced losses of FIs from the plasma.
- The profiles of NC and FIDA signals averaged over individual bursts of MHD activity are well modelled by applying anomalous diffusion to the FIs in NUBEAM.
- Fishbones strongly affect the high-energy, passing FI population in a manner which may be reproduced with some success using the fishbone model in NUBEAM.

The results presented in this paper demonstrate the advantages of employing several complementary diagnostics to study the behaviour of the FI population. Extending previous studies on the MAST [7, 23, 24, 32], a systematic analysis of NC and FIDA data has allowed the deleterious effects of chirping TAEs and fishbones on the confined FI population to be identified with confidence. The velocity-space sensitivity of the FIDA measurements, moreover, permits losses of FIs to be identified unambiguously, and these losses are seen to be strongly correlated with the MHD activity.

Radial profiles of neutron and FIDA emission have been used to constrain transport modelling and to establish the effects of fishbones on the FI distribution. A simultaneous comparison of the modelling results to measurements made with the FC, NC and FIDA diagnostics has allowed constraints to be placed on the effects of fishbones on the velocity-space distribution of FIs; these modes are seen to affect high-energy, passing particles in the core of the plasma. Data from the

prototype CFPD support the conclusion that fishbones have a strong impact on core FI confinement. The shortcomings of the basic diffusive and fishbone-loss models available to simulate anomalous FI transport in the TRANSP code have been revealed by confronting each of these models with data from multiple FI diagnostics.

The additional flexibility offered by the NBI system on the forthcoming MAST-Upgrade device, which will have the capability to inject beams simultaneously on and off-axis, will allow a detailed investigation into the relationship between beam deposition profiles, MHD mode activity and FI transport [32].

Acknowledgments

This work was part-funded by the RCUK Energy Programme under grant EP/I501045, by the Swedish Research Council, and by EURATOM. To obtain further information on the data and models underlying this paper, please contact PublicationsManager@ccfe.ac.uk. The views and opinions expressed herein do not necessarily reflect those of the European Commission.

References

[1] Pinches S D *et al* 2004 The role of energetic particles in fusion plasmas *Plasma Phys. Control. Fusion* **46** B187–200
[2] Akers R J *et al* 2003 Transport and confinement in the mega ampère spherical tokamak (MAST) plasma *Plasma Phys. Control. Fusion* **45** A175–204
[3] Buttery R J *et al* 2004 Stability at high performance in the MAST spherical tokamak *Nucl. Fusion* **44** 1027–35
[4] Gee S J *et al* 2005 MAST neutral beam long pulse upgrade *Fusion Eng. Des.* **74** 403–7
[5] Mikhailovskii A B 1975 Thermonuclear 'drift' instabilities *Sov. Phys.—JETP* **41** 890–4
[6] Breizman B N, Berk H L and Ye H 1993 Collective transport of alpha particles due to Alfvén wave instability *Phys. Fluids* B **5** 3217–26
[7] Cecconello M *et al* 2015 Energetic ion behaviour in MAST *Plasma Phys. Control. Fusion* **57** 014006
[8] Pinches S D *et al* 2012 TH/P3-34: Development of a predictive capability for fast ion behaviour in MAST *Proc. 24th IAEA Fusion Energy Conf.* TH/P3–34
[9] http://w3.pppl.gov/transp, accessed 04/11/2014
[10] Pankin A, McCune D, Andre R, Bateman G and Kritz A 2004 The tokamak Monte Carlo fast ion module NUBEAM in the national transport code collaboration library *Comput. Phys. Commun.* **159** 157–84
[11] Perez R V *et al* 2014 Investigating fusion plasma instabilities in the mega amp spherical tokamak using mega electron volt proton emissions *Rev. Sci. Instrum.* **85** 11D701
[12] Stammers K and Loughlin M J 2006 The calibration of the MAST neutron yield monitors *Nucl. Instrum. Methods Phys. Res.* A **562** 521–30
[13] Cecconello M *et al* 2014 The 2.5 MeV neutron flux monitor for MAST *Nucl. Instrum. Methods Phys. Res.* A **753** 72–83
[14] Michael C A *et al* 2013 Dual view FIDA measurements on MAST *Plasma Phys. Control. Fusion* **55** 095007
[15] Hsu C T, Cheng C Z, Helander P, Sigmar D J and White R 1994 Particle dynamics in chirped-frequency fluctuations *Phys. Rev. Lett.* **72** 2503–7
[16] Mynick H E and Pomphrey N 1994 Frequency sweeping: a new technique for energy-selective transport *Nucl. Fusion* **34** 1277–82
[17] Breizman B N, Berk H L, Pekker M S, Porcelli F, Stupakov G V and Wong K L 1997 Critical nonlinear phenomena for kinetic instabilities near threshold *Phys. Plasmas* **4** 1559–68
[18] McGuire K *et al* 1983 Study of high-beta magnetohydrodynamic modes and fast-ion losses in PDX *Phys. Rev. Lett.* **50** 891–5
[19] Heidbrink W W and Sager G 1990 The fishbone instability in the DIII-D tokamak *Nucl. Fusion* **30** 1015–25
[20] Fredrickson E D *et al* 2003 Wave driven fast ion loss in the national spherical torus experiment *Phys. Plasmas* **10** 2852
[21] Nave M F F, Campbell D J, Joffrin E, Marcus F B, Sadler G, Smeulders P and Thomsen K 2011 Fishbone activity in JET *Nucl. Fusion* **31** 697–710
[22] Dickey D A and Fuller W A 1979 Distribution of the estimators for autoregressive time series with a unit root *J. Am. Stat. Assoc.* **74** 427–31
[23] Jones O M, Michael C A, McClements K G, Conway N J, Crowley B, Akers R J, Lake R J and Pinches S D 2013 Fast-ion deuterium alpha spectroscopic observations of the effects of fishbones in the mega-ampere spherical tokamak *Plasma Phys. Control. Fusion* **55** 085009
[24] Turnyanskiy M, Challis C D, Akers R J, Cecconello M, Keeling D L, Kirk A, Lake R, Pinches S D, Sangaroon S and Wodniak I 2013 Measurement and control of the fast ion redistribution on MAST *Nucl. Fusion* **53** 053016
[25] Duong H H, Heidbrink W W, Strait E J, Petrie T W, Lee R, Moyer R A and Watkins J G 1993 Loss of energetic beam ions during TAE instabilities *Nucl. Fusion* **33** 749–65
[26] Heidbrink W W 1999 Beam-driven chirping instability in DIII-D *Plasma Phys. Control. Fusion* **37** 937–49
[27] Fredrickson E D *et al* 2006 Collective fast ion instability-induced losses in national spherical tokamak experiment *Phys. Plasmas* **13** 056109
[28] Klimek I, Cecconello M, Gorelenkova M, Keeling D, Meakins A, Jones O, Akers R, Lupelli I, Turnyanskiy M and Ericsson G 2015 TRANSP modelling of total and local neutron emission on MAST *Nucl. Fusion* **55** 023003
[29] Heidbrink W W *et al* 2014 Confinement degradation by Alfvén-eigenmode induced fast-ion transport in steady-state scenario discharges *Plasma Phys. Control. Fusion* **56** 095030
[30] Heidbrink W W *et al* 1986 Tangential neutral-beam-driven instabilities in the princeton beta experiment *Phys. Rev. Lett.* **57** 835–8
[31] Betti R and Freidberg J P 1993 Destabilization of the internal kink by energetic circulating ions *Phys. Rev. Lett.* **70** 3428–30
[32] Keeling D L *et al* 2015 Mitigation of MHD induced fast-ion redistribution in MAST and implications for MAST-Upgrade design *Nucl. Fusion* **55** 013021